Utility of Postmortem Autopsy via Whole-Body Imaging: Initial Observations Comparing MDCT and 3.0T MRI Findings with Autopsy Findings

Jang Gyu Cha, MD[1]
Dong Hun Kim, MD[1]
Dae Ho Kim, MD[2]
Sang Hyun Paik, MD[1]
Jai Soung Park, MD[1]
Seong Jin Park, MD[1]
Hae Kyung Lee, MD[1]
Hyun Sook Hong, MD[1]
Duek Lin Choi, MD[3]
Kyung Moo Yang, MD[4]
Nak Eun Chung, MD[4]
Bong Woo Lee, MD[4]
Joong Seok Seo, MD[4]

Index terms:
Computed tomography (CT)
Magnetic resonance (MR)
Whole-body imaging
Forensic autopsy

DOI:10.3348/kjr.2010.11.4.395

Korean J Radiol 2010;11:395-406
Received January 19, 2010; accepted after revision April 5, 2010.

[1]Department of Radiology, Soonchunhyang University Bucheon Hospital, Gyunggi-do 420-020, Korea; [2]Department of Radiology, Konyang University Hospital, Daejeon 302-718, Korea; [3]Department of Radiology, Soonchunhyang University Hospital, Seoul 140-743, Korea; [4]Department of Forensic Medicine, National Institute of Scientific Investigation, Seoul 158-707, Korea

This research was supported by the Research & Development Program for new technology of Forensic Pathology through the National Institute of Scientific Investigation (NISI) funded by the Ministry of Public Administration and Security (1315000226, NISI-NG-2010-1).

Address reprint requests to:
Kyung Moo Yang, MD, Department of Forensic Medicine, National Institute of Scientific Investigation, 331-1 Sinwol 7-dong, Yangcheon-gu, Seoul 158-707, Korea.
Tel. (822) 2600-4612
Fax. (822) 2600-4829
e-mail: rudany@korea.kr

Objective: We prospectively compared whole-body multidetector computed tomography (MDCT) and 3.0T magnetic resonance (MR) images with autopsy findings.

Materials and Methods: Five cadavers were subjected to whole-body, 16-channel MDCT and 3.0T MR imaging within two hours before an autopsy. A radiologist classified the MDCT and 3.0T MRI findings into major and minor findings, which were compared with autopsy findings.

Results: Most of the imaging findings, pertaining to head and neck, heart and vascular, chest, abdomen, spine, and musculoskeletal lesions, corresponded to autopsy findings. The causes of death that were determined on the bases of MDCT and 3.0T MRI findings were consistent with the autopsy findings in four of five cases. CT was useful in diagnosing fatal hemorrhage and pneumothorax, as well as determining the shapes and characteristics of the fractures and the direction of external force. MRI was effective in evaluating and tracing the route of a metallic object, soft tissue lesions, chronicity of hemorrhage, and bone bruises.

Conclusion: A postmortem MDCT combined with MRI is a potentially powerful tool, providing noninvasive and objective measurements for forensic investigations.

Forensic science has advanced in several fields, including genetics, crime scene investigation methods, and toxicology (1). In contrast, autopsies still use traditional methods, including the dissection of the corpse, oral description, photography of the body, and written documentation of the findings (2). However, a conventional autopsy has many limitations including subjectivity, lack of reproducibility, restrictions on investigating the entire body and for the inability of a layman to understand the complex autopsy results (3).

Due to the rapid development of magnetic resonance (MR) imaging and computed tomography (CT) over the course of recent decades, the territory of radiology has been extending from the brain, chest, and abdominal imaging to the heart and articular imaging. In contrast to the rapid development of clinical radiology, the application of imaging methods in forensic radiology has lagged far behind the technical developments in imaging devices (1). An effort to document the body by objective and noninvasive means began in the 1990s at the Institute of Forensic Medicine, Diagnostic Radiology, and Neuroradiology of the University of Bern. This effort resulted in the 'Virtopsy' project, which aimed to detect forensic findings in corpses using multidetector CT (MDCT) and MR imaging, as well as comparing these results with traditional autopsy findings (4).

Furthermore, with the advent of higher channel MDCT and 3.0T whole-body MRI,

the potential of forensic radiology has increased. Many studies have been performed to evaluate the utility of whole-body postmortem MRI in non-forensic cases for detecting gross cranial, thoracic, and abdominal disease (4–9). Other groups have already performed whole-body postmortem imaging with MDCT (10, 11).

However, none of these studies included systematic whole-body examinations using a combination of multidetector CT and MRI (4–9) for forensic purposes. The present study was designed to compare whole-body MRI findings at 3.0T and 16-channel MDCT for determining the cause of death, with autopsy findings as the reference standard.

MATERIALS AND METHODS

Subjects

Five cadavers were selected among the autopsy cases between February and March 2008. The imaging study was performed as a pre-evaluation process before the autopsy. The research proposal was approved by the Institutional Review Board and inclusion criteria required the cadavers to have been from individuals aged 18 years or older and who were suspected to die of unnatural causes. Exclusion criteria were lack of informed consent from the family, extreme injury, or putrefaction of the body. The study subjects included four men and one woman. Their ages ranged from 23 to 71 years (mean, 47.8 years). CT and MRI were performed within 6–24 hours after death. The corpses were draped with a vinyl cloth wrapper to prevent contamination of the machines due to any secretions or hemorrhage from the body.

CT Scanning

CT was performed on a 16-detector MDCT (Sensation 16; Siemens, Erlangen, Germany). The subjects were imaged in the supine position with arms up from the vertex to the toe in two spiral acquisitions. All images were acquired using 1.5-mm detectors with a table feed of 36 mm per rotation (pitch 1.5). The protocol for all scan acquisitions involved the use of a helical pitch of 0.532:1, 120 kVp, 160 mA, a 512 × 512 matrix, and a 0.5-s rotation time, with a 50-cm field of view (FOV). The images were reconstructed into 1-mm detector widths with both bony and soft tissue algorithms. Using a Leonardo workstation (Syngo CT software; Siemens), two-dimensional sagittal and coronal reformations, as well as three-dimensional (3-D) reconstructions were calculated. Multi-planar reformatted images were reviewed by using window widths of 1,500–8,000 and window levels of 500–2,000.

The reconstructed images were sent to an intradepartmental PACS (Star PACS; Infinite, Seoul, Korea) using the Digital Imaging and Communications in Medicine protocol. The duration of the MDCT scan in our cases was approximately 2–3 min.

MRI Scanning

Whole-body MRI examinations were performed on a 3T MR system (Signa HDx; GE Healthcare, Milwaukee, WI) using a body coil. Detailed parameters for imaging sequences are provided in Table 1. The corpses were placed in the supine position, with arms beside the body and examined from head to toe.

Coronal and sagittal images were obtained using a maximum FOV of 45–50 cm and a turbo short tau inversion recovery (STIR) through five stations in the coronal orientation: head/neck, thorax/abdomen, pelvis, thighs, and calves. Subsequently, the whole body was scanned with coronal and sagittal T1-weighted fast spoiled gradient-echo (FSPGR) sequences. Whole-body STIR

Table 1. MRI Parameters

Station \ Parameter	Pulse Sequence	TE (ms)	TR (ms)	TI (ms)	FA	BW (kHz)	FOV (cm)	Thickness/ Spacing (mm)	Matrix	NEX	Scan Time
1	FSPGR	2.1	180		80	62.5	48	8/2	256×192	1	0:36
	STIR	27	4,000	180	90	62.5	48	8/2	256×224	1	3:37
2	FSPGR	2.1	180		80	62.5	48	8/2	256×192	1	0:37
	STIR	27	4,000	180	90	62.5	48	8/2	256×224	1	3:37
3	FSPGR	2.1	180		80	62.5	48	8/2	256×192	1	0:37
	STIR	27	4,000	180	90	62.5	48	8/2	256×224	1	3:37
4	FSPGR	2.1	180		80	62.5	48	8/2	256×192	1	0:41
	STIR	27	4,000	180	90	62.5	48	8/2	256×224	1	3:37
5	FSPGR	2.1	180		80	62.5	48	8/2	256×192	1	0:41
	STIR	27	4,000	180	90	62.5	48	8/2	256×224	1	3:37

Note.— BW = bandwidth, FA = flip angle, FOV = field of view, FSPGR = fast spoiled gradient-recalled turbo, NEX = number of excitations, STIR = short tau inversion recovery, TE = echo time, TI = inversion time, TR = repetition time

imaging was possible within 12–28 min and T1-weighted imaging within 10–16 min at a 1.3 × 1.1 mm and 1.8 × 1.3 mm in-plane resolution, respectively. Total imaging time for whole-body imaging was less than 40 min in all cases. If major findings were detected on whole-body images or an external wound was found on a part of the body, closer investigations were performed with dedicated local coils (head coil, surface coil, shoulder coil) (Table 2).

After the examination, the images were electronically aligned to one image of the whole body in the coronal and sagittal plane using commercial software.

Image Interpretation

A board-certified radiologist with six years of experience in reading musculoskeletal images prospectively reviewed whole-body CT and MR images, which were then referred to a cardioradiologist, chest radiologists, abdominal radiologists, a neuroradiologist, and a head and neck radiologist, and proceeded to analyze the radiological data with a focus on their subspecialties. They each performed their evaluations blinded to the autopsy findings and the photographic documentation. However, a forensic pathologist participated in CT and MR image acquisition and described each corpse's identity and the scenes of the accidents to radiologists. Initially, each radiologist independently completed detailed imaging data sheets with records made of the radiological findings. Radiological findings were then classified as major, directly associated with the cause of death, or minor, incidental findings (10, 12). The main findings provided in the autopsy summary report as being the relevant basis for the cause of death were compared to the results of the radiological evaluation. The

Table 2. List of MRI Coils Used in This Study

Case	Main Coil	Additionally Used Coils	Additionally Used Sequences
1	Body coil	8 channel head coil & 8 channel Cardiac Array	Axial T2 weighted imaging, gradient sequences for cardiac scan
2	Body coil	8 channel head coil & 8 channel Torso Array	Axial and coronal T2 weighted sequence for brain and pelvis
3	Body coil	8 channel head coil & 8 channel Torso Array	Axial and coronal T2 weighted sequence for brain and pelvis
4	Body coil	8 channel Neurovascular Array	Axial and coronal T1 and T2 weighted sequence for brain, neck
5	Body coil	8 channel Neurovascular Array- & 8 channel Torso Array	Axial and coronal T1 and T2 weighted sequence for brain

Table 3. Comparison of Multidetector CT, 3.0T MRI and Autopsy: Major Findings

Case	Major Findings		
	Multidetector CT	MRI	Autopsy
1	Cardiomegaly	Hypertrophy of left ventricular wall	Cardiomegaly
		Luminal narrowing of LAD*	Severe CAS
			Hypertrophy of left ventricular free wall
2	Collapse of abdominal aorta and IVC	Curvilinear metallic artifact through	Injury of right femoral artery & vein
	Absence of pulmonary edema	right thigh and psoas muscle	with SCH
	Soft tissue defect on medial aspect		Pale internal organ
	of right thigh		Absence of pulmonary edema.
3	Multiple rib fractures	Multiple rib fractures	Multiple rib fractures
	Fracture of C4	Fracture of C4	Fracture of C4
	Pneumo- and hemothorax, right with	Pneumo- and hemothorax with	Pneumo- and hemothorax
	mediastinal shift	mediastinal shift	Rupture of right lung
	Rupture of liver	Rupture of liver	Rupture of liver
	Hemoperitoneum	Hemoperitoneum	Hemoperitoneum
4	Left temporal bone fracture	Muscle contusion in left temporal area	Left temporal bone fracture
	SAH	SAH	IMH in left temporalis muscle
			SAH
5	Occipital and parietal bone fracture	ICH	Occipital, parietal and frontal bone
	ICH, left	SAH	fracture
	SAH		Cerebral contusion and SAH, ICH

Note.— * Radiologic findings in MR images used by local coil.
CAS = coronary atherosclerosis, ICH = intracranial hemorrhage, IMH = intramuscular hemorrhage, IVC = inferior vena cava , LAD = left anterior descending coronary artery, SAH = subarachnoid hemorrhage, SCH = subcutaneous hemorrhage

process of radiological evaluation, which involved determining whether a radiological finding should be included in the cause of death and be classified as major or minor, was decided by a radiologist after close consultation with each subspecialist. The CT and MRI findings were compared to the findings documented in the autopsy protocols and used as the reference standard.

Autopsy

An autopsy was performed, within 2 hours after imaging by a certified pathologist with at least 10 years of experience in forensic pathology, according to the standard protocol. The pathologist performing the autopsies was blinded to the CT and MRI findings. Routine formal dissection of the cranium, thorax, and abdomen, including the bowel and viscera, was undertaken in the five corpses. When the autopsy procedure was performed, the extent of dissection was decided by the forensic pathologist. Cause of death, primary illnesses, associated illnesses, and incidental findings were then recorded. Findings at CT and MRI were then correlated with the autopsy findings.

Table 4. Comparison of Multidetector CT, 3.0T MRI and Autopsy: Minor Findings

Case	Minor Findings		
	Multidetector CT	MRI	Autopsy
1	None	Tear of deltoid muscle	SCH on right deltoid muscle
2	Tear of right psoas muscle	Tear of right psoas muscle	Subendocardial hemorrhage of left ventricle
3	Crainoplasty on right temporal bone	Old hemorrhage in right temporal lobe*	Old hemorrhage in right temporal lobe
	Fracture of spinous processes of C3-5	Fractures in C3-5, T7, T8, L1	Crainoplasty on right temporal bone
	Compression fractures in T7, L1	Bone bruise in T2, T3	Fractures of spinous processes of C3-5
	Fracture of right pelvic bone	SCH in lower back back	Fractures in T7, T8, L1
	Intramuscular emphysema in right abdominal wall	Contusion in left side chest wall left forearm	Fracture of right pelvic bone
			SCH in upper and lower back
	Left hip dislocation	Left hip dislocation	Avulsion injuries of left elbow and knee
			SCH in extremities
			Left hip dislocation
4	Pneumocephalus due to injury of petrous bone with obliteration of mastoid air cell	SGH on left occipital bone	Hemorrhage in left petrous bone
			SGH on left occipital area
			SCH & IMH in anterior neck
	SGH on left occipital bone		Fracture in thyroid cartilage
			SCH & IMH of trapezius muscle
			Mild CAS in LAD
5	Left SGH	Left SGH*	SGH in occipital region
	Calcification on LAD	SCH & IMH in scapular area gluteus maximus muscle	SCH & IMH in scapular area and gluteus maximus muscle
		Baker's cyst in knee joint	Baker's cyst in knee joint
			Severe CAS

Note.— * Radiologic findings in MR images used by local coil
CAS = coronary atherosclerosis, IMH = intramuscular hemorrhage, LAD = left anterior descending coronary artery, SCH = subcutaneous hemorrhage, SGH = subgaleal hemorrhage

Table 5. Comparison of Multidetector CT, 3.0T MRI and Autopsy: Causes of Death

Case	Cause of Death		
	CT	MRI	Autopsy
1	None	Suspected ischemic heart disease	Ischemic heart disease
2	Hypovolemia due to massive hemorrhage	Hypovolemia due to massive hemorrhage	Hypovolemia due to injury of femoral vessels
3	Tension pneumothorax	Tension pneumothorax	Injury of multiple organs
	Massive hemorrhage	Massive hemorrhage	
4	Traumatic head injury	Suspected traumatic head injury	Traumatic head injury
5	Spontaneous intracranial hemorrhage	Spontaneous intracranial hemorrhage	Spontaneous intracranial hemorrhage

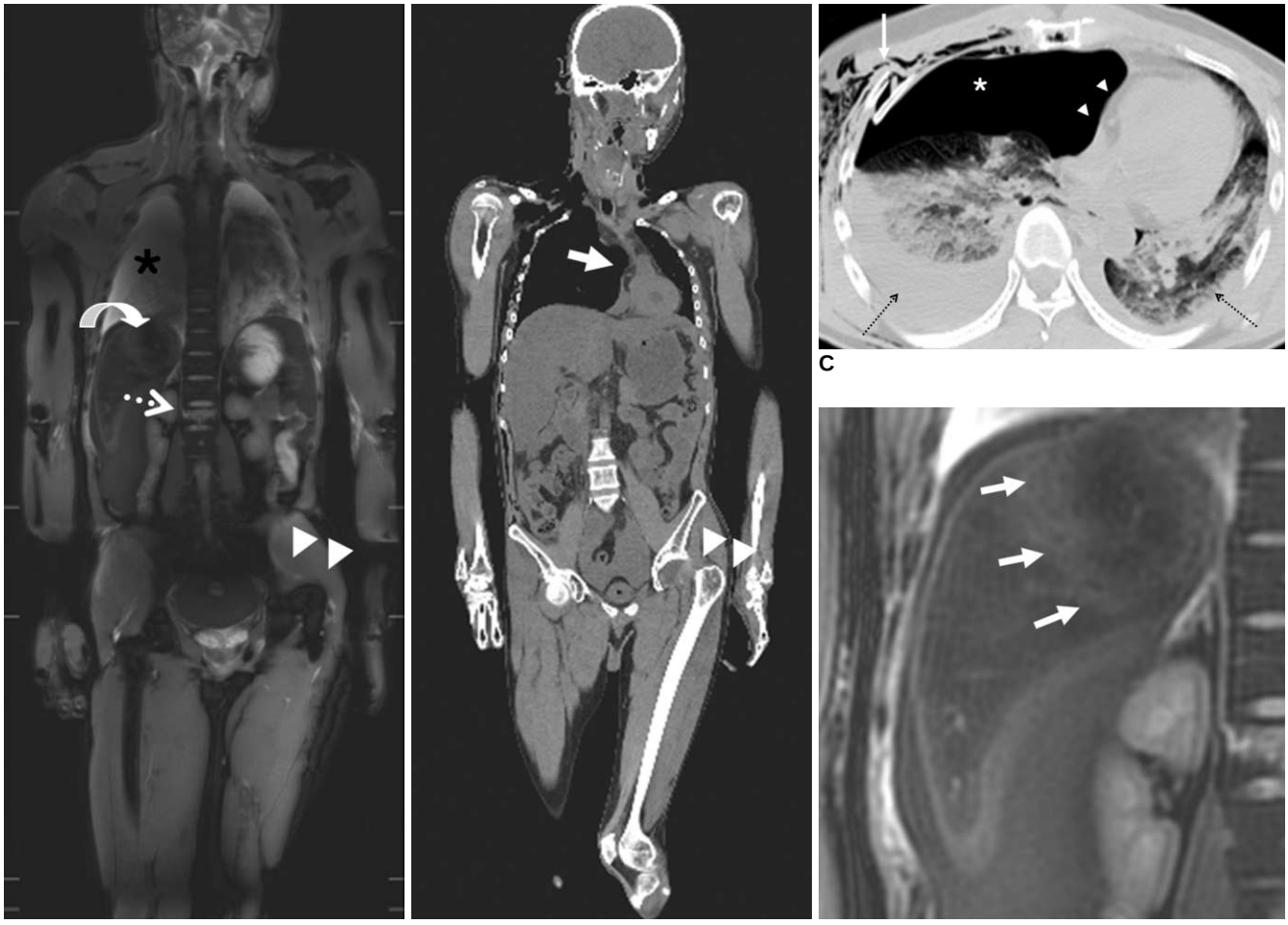

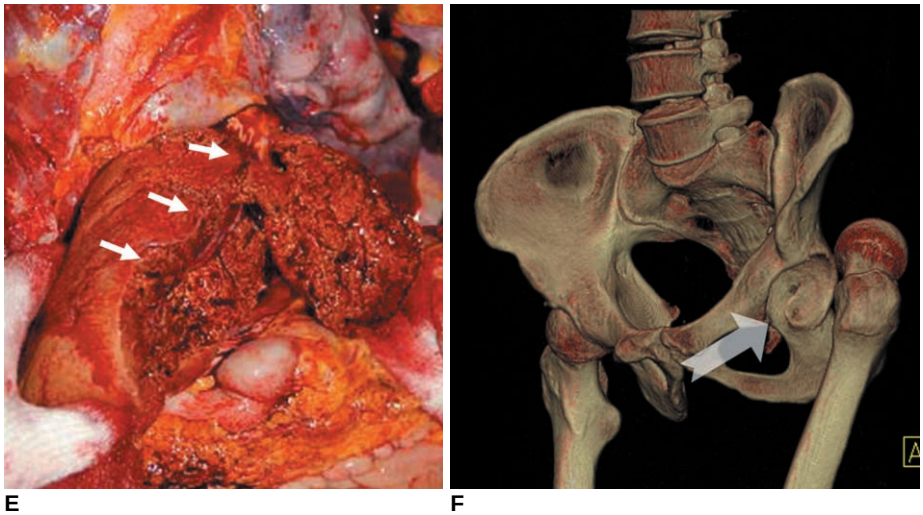

Fig. 1. 40-year-old man (pedestrian) who died in motor vehicle accident.
A. Coronal short tau inversion recovery whole-body MR image shows collapse of right lung (asterisk), low signal intensity lesion in right lobe of liver (curved arrow), high signal intensity lesion in L1 vertebral body (dashed arrow), and posterior dislocation of left hip joint (arrowheads).
B. Coronal reformatted whole-body CT image showing mediastinal shifting to left side (arrow) and posterior dislocation of left hip joint (arrowheads).
C. Axial thoracic CT with lung setting showing subcutaneous emphysema and right rib fracture with inferior displacement (solid arrow). Bilateral pleural effusions are also seen (dashed arrows). Mediastinal shifting (arrowheads) to left side caused by pneumothorax (asterisk), which could not be detected after opening thoracic cavity in conventional autopsy.
D. Magnified image of liver from (**A**) shows low signal lesion with intermediate signal intensity margin in right lobe of liver, suggesting traumatic rupture of liver (arrows).
E. Corresponding pathological photograph confirms rupture of right lobe of liver (arrows).
F. Volume-rendered CT image shows posterior dislocation of left hip joint, suggesting that external force was applied in anteroposterior direction (arrow).

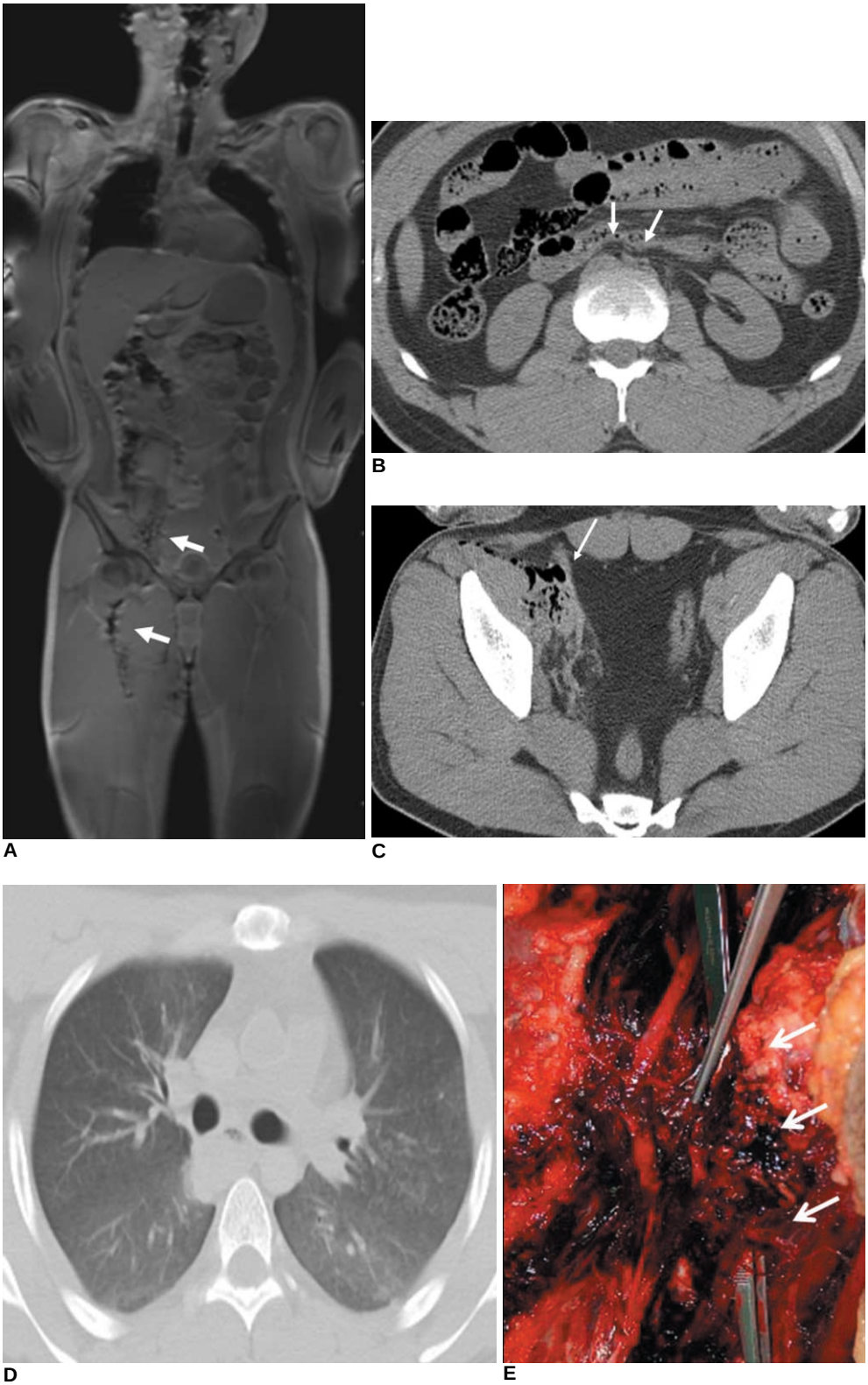

Fig. 2. 23-year-old man whose right thigh was pierced by iron bar.
A. Coronal T1 fast spoiled gradient-echo image shows curvilinear streaky lesion (arrows) along right thigh and psoas muscle caused by susceptibility artifact, which can help determine path of iron bar in body.
B. Axial CT image of pelvis demonstrates collapse of abdominal aorta and inferior vena cava (arrows).
C. Axial CT image of pelvis at acetabular level shows loculated air collection along right iliac vessels (arrow).
D. Lung window view of transverse CT scan shows absence of any increased density in lung parenchyma.
E. Autopsy photography reveals forceps putting through pathway of iron bar (arrows) and ruptured right femoral artery (holded by forceps) located within this pathway.

RESULTS

The major and minor findings are summarized in Tables 3 and 4, respectively. Cause of death based on CT and MRI findings agreed with those based on autopsy findings in four of the five cases (Table 5). In the other case, ischemic heart disease (IHD) was suspected as the potential cause of death based on MR images.

Head and Neck

Intracranial lesions were detected in three cases. In the third case, the CT scan revealed that the patient had undergone a cranioplasty on the temporal bone. The MRI scan revealed the late stages of subarachnoid hemorrhage on the surface of the temporal lobe. In the fourth case, the CT scan showed a temporal bone fracture, fracture of the petrous region, and diffuse subarachnoid hemorrhage, but the MRI scan failed to detect the temporal bone fracture (Fig. 3). In the fifth case, an intracerebral hemorrhage was demonstrated in MRI and CT scans, but only the CT scan revealed the actual extent of the fracture, which extended to the occipital, parietal, and frontal bone.

Thorax

In one case (case 3), mediastinal shift was observed to the left side, which was caused by pneumothorax, with multiple rib fractures on CT and MRI scans (Fig. 1A–D). The CT scan showed subcutaneous emphysema along the outside of the right chest wall (Fig. 1B, C).

Heart and Great Vessels

In one case (case 1), where the cause of death was confirmed to be IHD with severe atherosclerotic changes and hypertrophy of the left ventricular wall, MRI showed hypertrophy of the left ventricular wall on T2-weighted images. As no additional findings supported IHD, we classified IHD as only a potential cause of death in this case. CT images showed coronary calcifications in two cases (cases 1, 5).

In one case (case 2), CT and MR images showed obliteration of the vessels in the thigh and inguinal area and a curvilinear metallic artifact (Fig. 2A), collapse of the abdominal aorta and inferior vena cava (Fig. 2B), and the absence of any increased density in the lung parenchyma (Fig. 2C), indicating a massive hemorrhage due to vascular injury of the femoral vessels; this was confirmed by the autopsy findings (Fig. 2D, E).

Abdomen

In the third case, both CT and MRI showed a liver laceration in the right lobe of the liver with intraperitoneal hemorrhage, which was consistent with the autopsy findings (Fig. 1E, F).

Spine and Extremities

CT missed one fracture (T8) and MRI detected all six vertebral fractures (C3-5, T7, T8, and L1) confirmed by autopsy in case 3 (Fig. 1A). In contrast, STIR images revealed high signal intensity lesions in the second and third thoracic vertebral bodies, suggesting a vertebral contusion seen as a geographic area of nonlinear, increased signal intensity on bone marrow, which was not found by the autopsy. In the same corpse, the CT and MR images demonstrated that the femoral head was dislocated posteri-

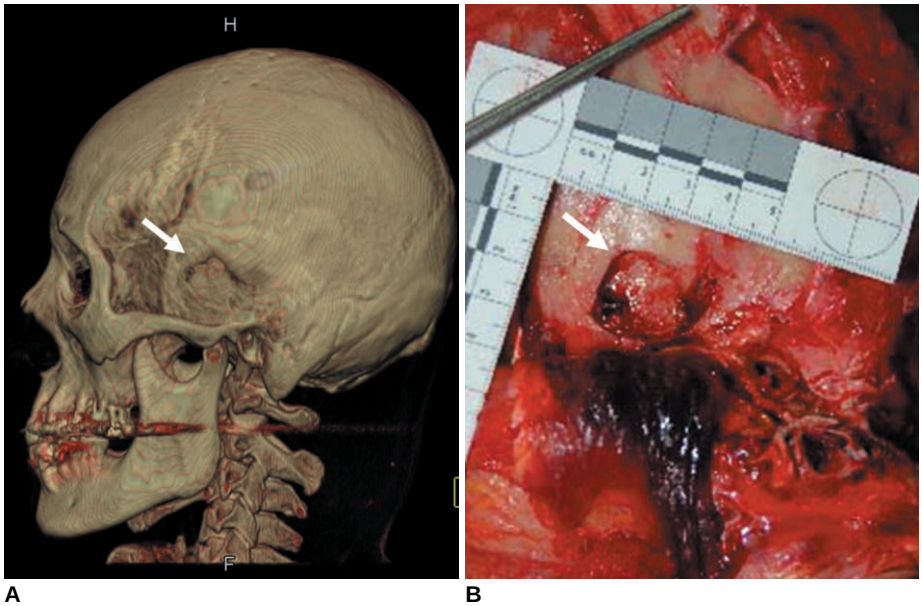

A B

Fig. 3. 57-year-old man who died due to head injuries from hammer.
A. Volume-rendered CT image of skull shows round depressive fracture in left temporal bone (arrow).
B. Autopsy photograph of left temporal bone shows similar size and shape of depressed fracture (arrow) which was observed in CT image.

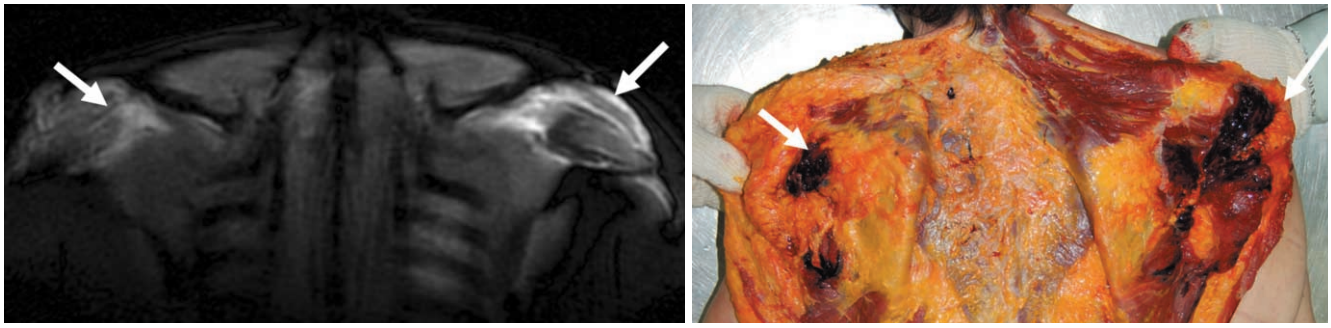

A B

Fig. 4. 71-year-old woman who fell from chair after spontaneous intracranial hemorrhage.
A. Coronal STIR images show increased signal intensity along posterior subcutaneous area of both scapular regions (arrows).
B. Autopsy photography of upper back reveals fresh soft tissue hemorrhage in corresponding areas (arrows).

orly from the acetabulum of the pelvic bone (Fig. 1F). MRI detected seven of 12 soft tissue injuries confirmed by autopsy (58%) (Fig. 4).

DISCUSSION

While the traditional autopsy is considered the gold standard for postmortem investigation, it has several obvious limitations. First, it is subjective and operator-dependent (3). Second, in cases when an important clue in a crime is newly discovered, a new interpretation of corpse injuries based on that clue may be required. However, such follow-up reviews of the corpse have to depend on written documents and selected parts or a small specimen retained for histological examination because the rest of the body tissues may have already been disposed of (3). Third, in the absence of advanced information, an autopsy may miss a traumatic injury of the extremities with no external wounds and lesions that are difficult to access by surgical dissection, such as injuries of the middle ear cavity. Finally, understanding the documentation of autopsy findings is often difficult for the layperson. Over the past decade, forensic radiology has challenged the conventional autopsy as a tool for objective, nondestructive documentation of the relevant forensic findings.

Since the first report by Wüllenweber et al. (13) in 1977 about the CT imaging of cranial bullet wounds, clinical radiological methods have been performed for forensic purposes. Although conventional X-rays have been frequently used in daily forensic practice, the practical application of newer, clinically established methods such as CT and MRI seem to have fallen behind in forensics (1). The 'Virtopsy' project was designed to integrate the conventional autopsy with advanced imaging technology, including MDCT and whole-body 3.0T MRI (1).

Although there have been many reports regarding postmortem MRI (5–9), few have focused on forensic or non-perinatal cases. Patriquin et al. (8) previously reported preliminary experiences of postmortem whole-body magnetic imaging in non-forensic cases. In their study, discrepancies between the causes of death determined by autopsy and MRI occurred in five of eight cases.

In four of five cases (80%), our results showed good consistency between radiological and autopsy findings in determining the cause of death, which represents a higher level accuracy than in the previous report. CT and MRI had a similar level of accuracy in deciding on the cause of death. In detail, CT imaging could provide a reliable diagnosis for traumatic head injuries, while MRI findings suggested the possibility of ischemic heart disease.

Whole-Body CT Imaging

CT is valuable for detecting osseous findings, foreign bodies, air embolisms, and gross abnormalities in soft tissue (11). Isotropic data can be obtained with far-advanced MDCT technology, which allows for high-resolution multiplanar reconstruction (14, 15). MDCT can be used to first perform a rapid, full-body screen to determine areas of particular forensic interest. Then, imaging data obtained from a whole-body CT scan can be reconstructed in all directions, allowing for a complete understanding of the characteristics of fractures developed from external injuries.

A larger FOV and faster acquisition times with high resolution can be achieved using 16-detector scanners. Indeed, the CT scanning time from the head to the knee was less than 3 min. In our study, CT was found to be superior to MRI in detecting skull fractures, which is consistent with a previous report (3).

Multidetector CT imaging had some advantages over MRI in detecting osseous injuries, including fractures and dislocations (1), as well as in assessing pneumothorax and fatal hemorrhage.

Detecting small fractures of some bones deeply seated in

the body, such as the spine, is difficult (1): Our results showed that MDCT imaging could detect several occult fractures in the skull, spine, and extremities with multiplanar reconstruction. In addition, isotropic imaging using 3-D reconstruction algorithms, such as a volume-rendering technique, can be used to display complex fractures and dislocations (4). In analyzing the cause of skull fractures, determining whether the fracture was the result of a fall to the ground or a blow to the head is an important forensic issue when a deceased person is initially found lying injured on the ground. This determination can be made on the basis of typical skull fracture systems, the morphological features of the crush wound, and contre-coup lesions within the brain (4). 3-D volume-rendered CT imaging in the fourth case showed a typical local impression in the temporal bone of the skull, suggesting the fracture was caused by blows from a hammer.

As shown in Figure 1F, the identification of a posterior hip dislocation allowed for an accurate determination of the direction of impact, demonstrating an advantage of virtual over conventional autopsy techniques.

Tension pneumothorax is difficult to detect by an autopsy because pathologists will likely miss the mediastinal shift at the moment the chest cavity is opened (1, 16). In our study, the CT images from case 3 showed a collapse of the lung parenchyma, with a mediastinal shift and rib fractures piercing the chest wall. CT scanning also showed extensive soft tissue emphysema along the chest wall, indicating that ventilation persisted for some time after the accident (4).

To date, little is known about the radiological findings in death by fatal hemorrhage. In the absence of massive external bleeding, large amounts of blood in either the thoracic or abdominal cavity can be readily detected by imaging (16). In cases of massive bleeding, the intense pallor of internal organs is a characteristic finding suggesting the extensive hemorrhage detected only upon pathological inspection; this finding cannot be detected by CT or MR images (16). As shown in Figure 2, and as suggested by Thali et al. (16), if massive bleeding occurs, a collapse of the descending aorta may be a reproducible radiological sign of massive or even fatal hemorrhage. In addition, pulmonary edema is known as an associated postmortem change (17). Two mechanisms proposed for postmortem pulmonary edema are a pressure gradient between the pulmonary vasculature and the alveolar spaces and changes in capillary permeability (17). We believe that in addition to the collapse of the descending aorta, the absence of pulmonary edema can be another sign that supports fatal hemorrhage in CT imaging, which is shown as diffusely increased opacity in lung parenchyma with a lung window setting.

Whole-Body MRI

Whole-body MRI is becoming increasingly common in the field of oncological imaging as an adjunct or alternative to established multimodal approaches (e.g., radiographs, MDCT, ultrasound, scintigraphy) in the initial tumor staging or screening for tumor recurrence after curative therapy (18). Furthermore, in whole-body MRI, the gain in the signal-to-noise ratio can be used to reduce the overall scan time, especially for the acquisition of T2-weighted, fat-suppressed sequences at a constant image resolution using 3.0T MRI (19). The main pulse sequences used in our study were FSPGR and turbo STIR imaging, which have proven to be effective for evaluating soft tissue and bone structures (15).

A large gap between the contiguous sections and limited coverage of the body has been the major obstacle to the close investigation of the body in imaging. In our study, we indicated the technical superiority of whole-body MRI at 3.0T, over preliminary studies, including an overall increased signal-to-noise ratio, no gap between sections, and full coverage of the body from head to toe. The scan time for whole-body MRI in our study was less than 40 min, and permitted high-quality imaging resolution. Except for specific organs, such as the brain and heart, for which MRI with multichannel multi-coil systems is required to fully exploit the 3.0T potential, the 3.0T whole-body MRI provides high spatial resolution images for screening of the whole body in forensic pathology, including areas that are not opened in routine autopsy procedures. In the near future, the scan time for the whole body may be considerably reduced by parallel imaging, which may lead to the widespread use of whole-body MRI in forensic investigations.

Yen et al. (3) reported that MRI and CT had the potential to play important roles in future forensic neuropathological examinations. Indeed, our results showed, in two cases (cases 4, 5), that MRI and CT imaging were equally effective in evaluating intracranial hemorrhages, including intracerebral, subarachnoid, and intraventricular hemorrhages (3). In particular, as shown in case 3, MRI revealed an old hemorrhage in the right temporal lobe, which was not seen by CT imaging. Gradient-echo MRI may be more effective in finding traces of old hemorrhages than conventional spin-echo imaging (20).

The pathology of subcutaneous fatty tissue, which is vulnerable to blunt trauma, can be clearly seen in MRI. MRI is also regularly used in the assessment of victims that survived blunt trauma, especially in cases of manual strangulation (21). Whole-body MRI helped detect

muscular and soft tissue lesions in cases 1, 3, and 5, which can be useful in determining the force of an impact (22) and also, the direction in some cases.

Detecting traumatic lesions in subcutaneous fat tissue is useful, as they can provide important clues in forensic investigations. Forensic radiology, based on advanced CT and MRI, can be performed noninvasively and objectively. Yen et al. (22) reported that MRI could determine mild subcutaneous lesions (perilobular hemorrhages).

In motor vehicle accidents, radiological methods have been used for identifying impact locations and directions in victims. In one subject (case 3), the pattern of massive destruction of fatty tissue and a huge subcutaneous cavity, in which blood and liquefied fat had collected, indicated that the victim had been run over by a car, as this type of trauma frequently accompanies being struck by the rotating wheel (4).

In clinical practice, MRI has susceptibility artifacts that are seen as signal voids and distortion in the presence of metal in an anatomical area of interest (23). In contrast, MRI using the susceptibility artifact has been used to detect intracranial hemorrhage (24).

As seen in our case 2, a metallic artifact on the MR images was seen from the inguinal area to the right common iliac artery, suggesting that a metallic object pierced the thigh along that trajectory. Thus, we believe that a metallic artifact in MRI can be effectively used to assess the direction from which a piercing wound was created by a metallic object in forensic science.

Both MDCT and MRI provided good images of vertebral body injury in our study. However, the CT scan missed one vertebral fracture. We speculated that the main reason for the false-negative CT reading was that we used a reconstructed thickness of 3 mm. Using a thinner reconstructed thickness may lead to a more accurate diagnosis of spinal fractures comparable to an MRI scan.

Finding bone bruising of the spine in a conventional autopsy seems to be difficult because the spine is not usually included in the routine protocol of forensic autopsy, and bone bruising may not be a major morphological abnormality. In case 3, the STIR imaging allowed the diagnosis of two vertebral contusions not accessible to other imaging modalities and normal forensic evaluation. Thus, we believe that MRI is a valuable means to delineate bone contusions, which can be a major forensic finding revealing the direction of impact (25).

In our study, CT and MRI failed to detect myocardial infarction in one case (case 1). Although the cause of death in that case was determined on the basis of severe stenosis of the coronary arteries and hypertrophy of the ventricle, no direct evidence of myocardial infarction was found, even at autopsy. The absence of myocardial pathology was due to a hyperacute ischemic insult, which is known to progress too fast to allow recognizable cellular changes and vital tissue reactions, including edema and necrosis in the surrounding myocardium. Thus, neither the imaging study nor autopsy, identified the pathology of the myocardium (26). According to Grabherr et al. (27), after the establishment of postmortem perfusion with paraffin oil and injection of an oily contrast agent, the vascular system can be investigated in detail and vascular abnormalities rendered visible. This method may be useful to increase the detection of ischemic heart disease

We recommend the simultaneous use of CT and MRI in postmortem whole-body imaging because both imaging modalities can complement each other effectively. However, some limitations exist in the forensic use of a CT scan together with an MRI scan, including the high cost and low availability of imaging modalities. For this reason, the use of a whole-body imaging technique is needed to allow for the screening of forensic lesions within a tolerable time frame. The increasing number of government-established institutes equipped with CT and MRI scanners will lower the cost in the near future.

Our study had several limitations. First, given the small number of cases, the findings of this study must be considered to be preliminary results. Further work with a larger sample size is needed to validate our findings. Second, a certain amount of subjective bias may have occurred because one radiologist had to determine the cause of death with each imaging modality, after obtaining advice from seven other subspecialty radiologists to aid in interpreting the CT and MRI findings. Third, the in-plane spatial resolution of whole body MR images in our study was not superior to such resolution in prior studies in which whole body MR imaging was used for clinical evaluation; the time available for postmortem MR imaging was restricted in our clinical institution. A dedicated MRI scan for forensic imaging might improve image resolution. Finally, there is the possibility of misinterpreting forensic findings because most of the radiologists participating in this study were not familiar with forensic radiology (8). However, recent studies have shown that the clinical radiological experience with CT and MRI can be applied to postmortem imaging (16). Several board certified reviewers collaborated in a review to bring more in-depth subspecialty expertise to the decision-making processes because it was too difficult for one radiologist to assess a variety of disease entities in the whole-body regions. Therefore, this review system allowed us to detect more detailed lesions throughout the whole body.

In conclusion, the results of this study indicate that

MDCT and MRI can noninvasively provide numerous forensic findings in a whole-body system on just one scan within a reasonable time. In addition, whole-body CT and MRI findings were quite consistent with autopsy findings; the major findings correctly indicated the cause of death in four of five cases. MDCT imaging with 3-D reconstruction is a rapid, useful tool for the diagnosis of skeletal fractures, pneumothorax with subcutaneous emphysema, and hypovolemia. MRI has advantages in detecting soft tissue lesions, bone bruising, hemorrhage, and tracing metallic objects or weapons in the body. Thus, postmortem whole-body CT and MRI are expected to do important roles as a screening and supplementary tests within the field of forensic medicine in short future.

Acknowledgment

The authors thank Byung Hun Yoo, Young Soo Kim, Sung Jin Kang, Myung Sik Joo, Jae Hwan Cho, Soo Han Chang, Yin Wan Cho, and Hyun Joo Kim for assistance during MRI and CT, imaging and Hyun Mu Kang, Hyung Nam Koo, Bon Young Koo, Ki Suk Kwon, Chun Do Ki, Dal Won Kim, Suk Kyung Kim, Won Jun Shu, You Jin Won, Young Seok Lee, Jong Seok Lee, Whee Yeal Cho, Ik Jo Chung, Jung Sick Chung, Gang Nam Jin in the division of forensic medicine, National Institute of Scientific Investigation, who endeavored to communicate, transfer, photograph, and assist in autopsies.

References

1. Bolliger SA, Thali MJ, Ross S, Buck U, Naether S, Vock P. Virtual autopsy using imaging: bridging radiologic and forensic sciences. A review of the Virtopsy and similar projects. *Eur Radiol* 2008;18:273-282
2. Lundberg GD. Low-tech autopsies in the era of high-tech medicine: continued value for quality assurance and patient safety. *JAMA* 1998;280:1273-1274
3. Yen K, Lövblad KO, Scheurer E, Ozdoba C, Thali MJ, Aghayev E, et al. Post-mortem forensic neuroimaging: correlation of MDCT and MRI findings with autopsy results. *Forensic Sci Int* 2007;173:21-35
4. Dirnhofer R, Jackowski C, Vock P, Potter K, Thali MJ. VIRTOPSY: minimally invasive, imaging-guided virtual autopsy. *Radiographics* 2006;26:1305-1333
5. Berry PJ, Keeling JW, Wigglesworth JS. Perinatal necropsy by magnetic resonance imaging. *Lancet* 1997;349:55
6. Brookes JA, Hall-Craggs MA, Sams VR, Lees WR. Non-invasive perinatal necropsy by magnetic resonance imaging. *Lancet* 1996;348:1139-1141
7. Woodward PJ, Sohaey R, Harris DP, Jackson GM, Klatt EC, Alexander AL, et al. Postmortem fetal MR imaging: comparison with findings at autopsy. *AJR Am J Roentgenol* 1997;168:41-46
8. Patriquin L, Kassarjian A, Barish M, Casserley L, O'Brien M, Andry C, et al. Postmortem whole-body magnetic resonance imaging as an adjunct to autopsy: preliminary clinical experience. *J Magn Reson Imaging* 2001;13:277-287
9. Ros PR, Li KC, Vo P, Baer H, Staab EV. Preautopsy magnetic resonance imaging: initial experience. *Magn Reson Imaging* 1990;8:303-308
10. Weustink AC, Hunink MG, van Dijke CF, Renken NS, Krestin GP, Oosterhuis JW. Minimally invasive autopsy: an alternative to conventional autopsy? *Radiology* 2009;250:897-904
11. Ross S, Spendlove D, Bolliger S, Christe A, Oesterhelweg L, Grabherr S, et al. Postmortem whole-body CT angiography: evaluation of two contrast media solutions. *AJR Am J Roentgenol* 2008;190:1380-1389
12. Grabherr S, Gygax E, Sollberger B, Ross S, Oesterhelweg L, Bolliger S, et al. Two-step postmortem angiography with a modified heart-lung machine: preliminary results. *AJR Am J Roentgenol* 2008;190:345-351
13. Wüllenweber R, Schneider V, Grumme T. A computer-tomographical examination of cranial bullet wounds (author's transl). *Z Rechtsmed* 1977;80:227-246 [German]
14. Dalrymple NC, Prasad SR, El-Merhi FM, Chintapalli KN. Price of isotropy in multidetector CT. *Radiographics* 2007;27:49-62
15. Groves AM, Beadsmoore CJ, Cheow HK, Balan KK, Courtney HM, Kaptoge S, et al. Can 16-detector multislice CT exclude skeletal lesions during tumour staging? Implications for the cancer patient. *Eur Radiol* 2006;16:1066-1073
16. Thali MJ, Yen K, Schweitzer W, Vock P, Boesch C, Ozdoba C, et al. Virtopsy, a new imaging horizon in forensic pathology: virtual autopsy by postmortem multislice computed tomography (MSCT) and magnetic resonance imaging (MRI)--a feasibility study. *J Forensic Sci* 2003;48:386-403
17. Durlacher SH, Banfield WG Jr, Bergner AD. Post-mortem pulmonary edema. *Yale J Biol Med* 1950;22:565-572
18. Schmidt GP, Reiser MF, Baur-Melnyk A. Whole-body imaging of the musculoskeletal system: the value of MR imaging. *Skeletal Radiol* 2007;36:1109-1119
19. Schmidt GP, Kramer H, Reiser MF, Glaser C. Whole-body magnetic resonance imaging and positron emission tomography-computed tomography in oncology. *Top Magn Reson Imaging* 2007;18:193-202
20. Tosaka M, Sato N, Hirato J, Fujimaki H, Yamaguchi R, Kohga H, et al. Assessment of hemorrhage in pituitary macroadenoma by T2*-weighted gradient-echo MR imaging. *AJNR Am J Neuroradiol* 2007;28:2023-2029
21. Yen K, Thali MJ, Aghayev E, Jackowski C, Schweitzer W, Boesch C, et al. Strangulation signs: initial correlation of MRI, MSCT, and forensic neck findings. *J Magn Reson Imaging* 2005;22:501-510
22. Yen K, Vock P, Tiefenthaler B, Ranner G, Scheurer E, Thali MJ, et al. Virtopsy: forensic traumatology of the subcutaneous fatty tissue; multislice computed tomography (MSCT) and magnetic resonance imaging (MRI) as diagnostic tools. *J Forensic Sci* 2004;49:799-806
23. Fidelman NA, Wilson MW, Bloom AI, Kerlan RK Jr, LaBerge JM, Gordon RL. Orthopedic spinal and hip prostheses: effects of magnetic susceptibility artifacts during MR arteriography and venography of abdomen and pelvis. *Radiology* 2006;240:894-899
24. Winkler ML, Olsen WL, Mills TC, Kaufman L. Hemorrhagic and nonhemorrhagic brain lesions: evaluation with 0.35-T fast MR imaging. *Radiology* 1987;165:203-207
25. Newberg AH, Wetzner SM. Bone bruises: their patterns and significance. *Semin Ultrasound CT MR* 1994;15:396-409
26. Jackowski C, Christe A, Sonnenschein M, Aghayev E, Thali MJ.

Postmortem unenhanced magnetic resonance imaging of myocardial infarction in correlation to histological infarction age characterization. *Eur Heart J* 2006;27:2459-2467
27. Grabherr S, Djonov V, Friess A, Thali MJ, Ranner G, Vock P, et al. Postmortem angiography after vascular perfusion with diesel oil and a lipophilic contrast agent. *AJR Am J Roentgenol* 2006;187:W515-W523